



Role of prism decussation on fatigue crack growth and fracture of human enamel

Devendra Bajaj^a, Dwayne Arola^{a,b,*}

^a Department of Mechanical Engineering, University of Maryland Baltimore County, 1000 Hilltop Circle, Baltimore, MD 21250, USA

^b Department of Endodontics, Prosthodontics, and Operative Dentistry, Baltimore College of Dental Surgery, University of Maryland, Baltimore, MD 21201, USA

Received 25 February 2009; received in revised form 3 April 2009; accepted 17 April 2009

Abstract

The role of prism decussation on the crack growth resistance of human enamel is evaluated. Miniature inset compact tension (CT) specimens embodying a section of cuspal enamel were subjected to Mode I cyclic or monotonic loads. Cracks were grown in either the forward (from outer enamel inwards) or reverse (from inner enamel outwards) direction and the responses were compared quantitatively. Results showed that the outer enamel exhibits lower resistance to the inception and growth of cracks. Regardless of the growth direction, the near-threshold region of cyclic extension was typical of “short crack” behavior (i.e. deceleration of growth with an increase in crack length). Cyclic crack growth was more stable in the forward direction and occurred over twice the spatial distance achieved in the reverse direction. In response to the monotonic loads, a rising R-curve response was exhibited by growth in the forward direction only. The total energy absorbed in fracture for the forward direction was more than three times that in the reverse. The rise in crack growth resistance was largely attributed to a combination of mechanisms that included crack bridging, crack bifurcation and crack curving, which were induced by decussation in the inner enamel. An analysis of the responses distinguished that the microstructure of enamel appears optimized for resisting crack growth initiating from damage at the tooth’s surface.

© 2009 Acta Materialia Inc. Published by Elsevier Ltd. All rights reserved.

Keywords: Decussation; DEJ; Enamel; Fatigue crack growth; Fracture

1. Introduction

Cyclic loading can cause the inception and growth of damage that reduces the “life” of engineering and biological materials [1]. The accumulation of cyclic damage often results in the generation of well-defined cracks that undergo subsequent growth and ultimately cause fracture under adequate driving forces and/or crack length [2–4]. Human teeth are susceptible to such fractures in the enamel crown [5], particularly in regions of the tooth that have

been restored [6]. While in tissues such as bone and cartilage the generation of microdamage and small cracks can be repaired by physiological processes [7], tissues of the tooth cannot undergo remodeling. They have been designed by nature to minimize the sensitivity to such defects and cracks [8,9]. In general, these materials achieve resistance to crack growth by the arrangement of their organic and inorganic constituents into densely packed hierarchical structures.

Human tooth enamel (Fig. 1a) is the most highly mineralized (96 wt.%) hard tissue of the body and is comprised of a comparatively low degree of organic matter (1 wt.%) and bound water (3 wt.%) [10]. It combines nanocrystals (~25 nm thick, ~100 nm wide and 500–1000 nm long) to form “keyhole”-shaped structures known as prisms (~4–8 μm in diameter). These prisms extend roughly perpendicular from the dentin–enamel junction (DEJ) towards the

* Corresponding author. Address: Department of Mechanical Engineering, University of Maryland Baltimore County, 1000 Hilltop Circle, Baltimore, MD 21250, USA. Tel.: +1 410 455 3310; fax: +1 410 455 1052.
E-mail address: darola@umbc.edu (D. Arola).

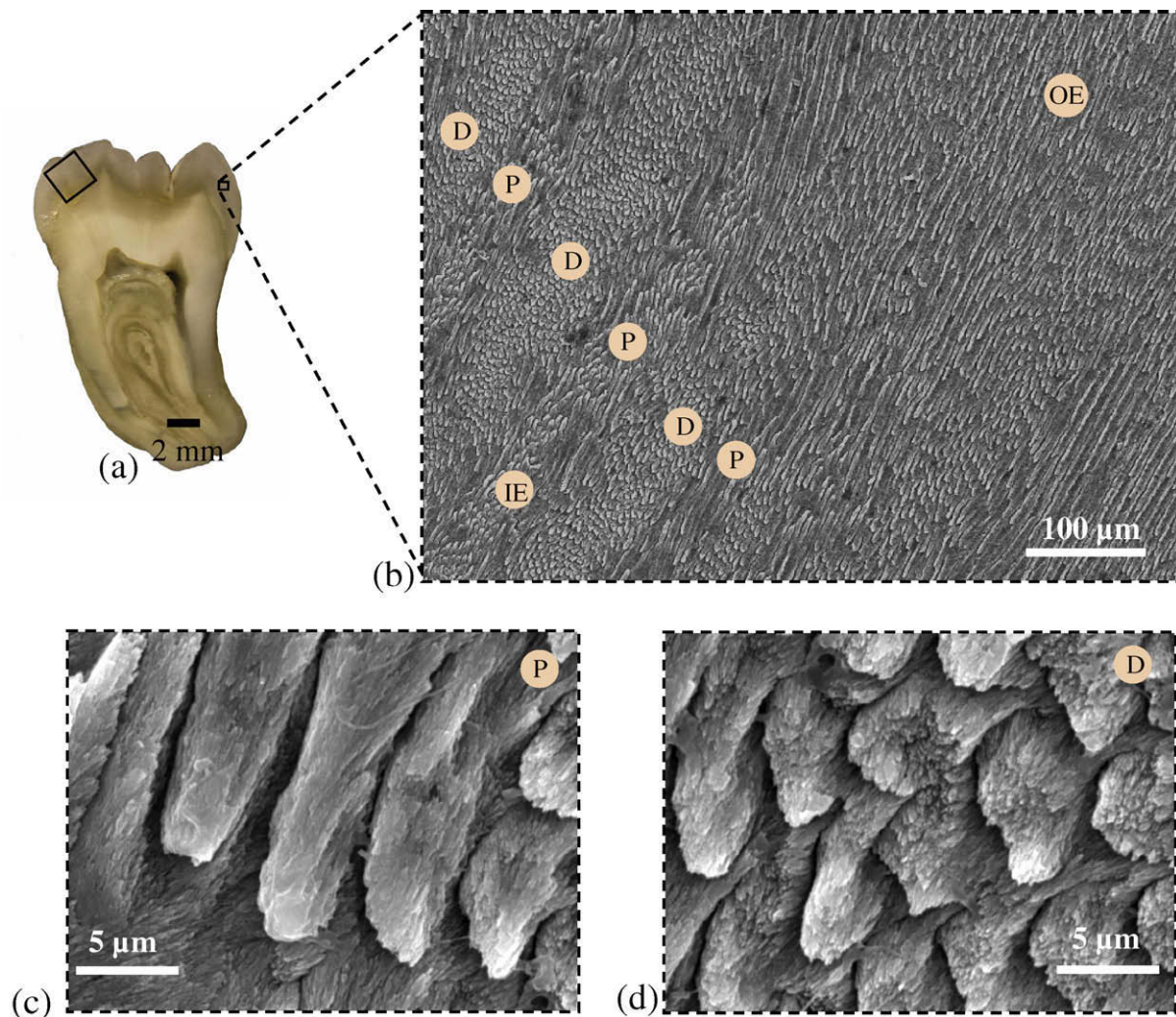


Fig. 1. Details pertaining to the microstructural arrangement of prisms in enamel. (a) A section of tooth and possible inset of enamel. (b) Distinction between the outer (OE) and the inner enamel (IE). Prisms are mostly oriented in a straight fashion in the outer enamel. Decussation, which is caused by crossing of prism bundles is mostly seen in the inner regions of the cuspal enamel and is comprised of bundles of prisms known as the parazone (P) and diazone (D) shown in (c) and (d), respectively.

surface of the tooth where they line up in a parallel fashion, essentially with their long axis perpendicular to the occlusal plane. The spaces between these tightly packed prisms are comprised of a non-collagenous organic matrix. It is the arrangement of these prisms that is responsible for the structural and the mechanical anisotropy in enamel, imparting greater toughness perpendicular to their longitudinal axis [11]. Natural cracks that develop in the enamel of human teeth are oriented along the long axis of the prisms [12], i.e. the direction with weakest resistance to extension [11]. This has raised questions concerning the microstructure of enamel and its role in achieving the necessary resistance to cracks extending from the tooth's surface inwards as well as those extending from the inner surface outwards.

There is presently little knowledge concerning the process of cyclic and monotonic crack growth in human enamel in comparison to that in bone (e.g. [13–17]) and dentin (e.g. [18–21]). While hydroxyapatite offers minimal

resistance to crack growth [22], the crossing of prism bundles in enamel imparts appreciable toughening [23,24]. Such features (Fig. 1b–d), known as decussation, are mostly seen in the inner regions of cuspal enamel [25]. Decussation has been identified in the enamel of many species [26,27] and the extent has been correlated with the magnitude of stresses that develop during mastication [28]. The high degree of decussation at or near the cusps results in greater surface area of prisms per unit volume [25], better crushing ability [29] and also might increase the resistance to fracture [24] by offering an “easy” (along the prisms) and a “difficult” (across the prisms) path for cracks to traverse. However, the contribution of this unique structure of enamel towards its crack growth resistance has not been explored in detail. Therefore, an evaluation of cyclic and monotonic crack growth in human enamel was conducted. Specifically, the role of decussation on crack growth resistance was examined by growing cracks in both forward and reverse directions.

2. Materials and methods

2.1. Specimen preparation

Unrestored third molars ($17 \leq \text{patient age} \leq 27$ years) were acquired from participating dental practices in Maryland according to an approved protocol by the Institutional Review Board of the University of Maryland Baltimore County. Small sections of enamel ($2 \times 2 \times 2 \text{ mm}^3$) were obtained from the cuspal region (Fig. 1a) using a slicing operation (K.O. Lee Model S3818EL, Aberdeen, SD, USA). Inset compact tension (CT) specimens (Fig. 2) were prepared by molding the enamel sections within a resin composite (Vit-I-escence, Ultradent Products, Inc., South Jordan, UT, USA). Detailed descriptions of bonding and placement of the inset have been described elsewhere [30,31]. All specimens were prepared to grow cracks parallel to the long axis of the prisms. The specimens were polished using particle suspension of sizes 9, 3 and $0.04 \mu\text{m}$ (Beuhler) with a standard cloth wheel. A back channel (1 mm deep) was introduced to avoid crack curving and two holes were drilled and counter-bored to enable Mode I cyclic loading (Fig. 2). Lastly, a chevron notch was prepared using a razor blade and diamond paste. Ten specimens were prepared to achieve crack growth from the outer enamel inwards (cyclic = 7, monotonic = 3), which is termed the “forward” path of crack extension. Cracks were also grown from the inner enamel outwards in 10 specimens (cyclic = 7, monotonic = 3), which is regarded as the “reverse” direction of extension.

2.2. Fatigue crack growth

All specimens were subjected to cyclic loading using an Enduratec Model ELF 3200 universal testing system. Crack initiation was achieved using a stress ratio (R) of 0.1 and frequency of 5 Hz with maximum load ranging from 3 to 6 N. Cyclic crack growth was then continued using the same protocol. The incremental crack growth rates (da/dN) were computed by dividing the measured

crack extension (Δa) over increments of growth (ΔN). Crack length measurements were achieved using a digital microscope (Navitar IEEE 1394) at a magnification of $42\times$. The stress intensity range (ΔK) was calculated using solutions obtained from a numerical model of the form:

$$\Delta K = \frac{\Delta P}{B^* \sqrt{W}} \sqrt{\frac{B^* + 1}{B + 1}} (1.69 - 8.01\alpha + 12.53\alpha^2) [\text{MPa m}^{0.5}], \quad (1)$$

where ΔP is the load amplitude, α is the ratio of a and W , B is the specimen thickness, and B^* is the specimen thickness within the back channel. Eq. (1) is valid for $2.0 \leq a \leq 3.6$, where the crack length (a) is measured from the crack tip to the center of the load line as shown in Fig. 2. The cumulative experimental responses obtained for each group were used to estimate the mean and standard deviation of specific growth parameters. The growth response was examined in terms of the absolute crack length from the notch (a_n).

2.3. Monotonic crack growth

Quasi-static loading of the selected precracked specimens was performed using a specially designed universal testing system complemented with a microscopic imaging system [30]. Prior to quasi-static loading, the specimen surfaces were coated with a very thin layer ($\sim 5 \mu\text{m}$ thick) of diluted correction fluid (used to erase typing errors) mixed with toner powder for application of micro digital image correlation (DIC). A detailed description of DIC and its application is given elsewhere [32]. Hydration of the samples during loading was achieved through a saturated cotton swab “cradle” that was nestled beneath the specimen and maintained moist with an eyedropper of Hanks’ Balanced Salt Solution (HBSS).

Opening mode loads were applied in increments of 1 N and less until the onset of crack extension was identified from decay in the load response. Thereafter, loading was continued in displacement control in 0.1 mm min^{-1} increments, followed by a dwell after each extension, and then

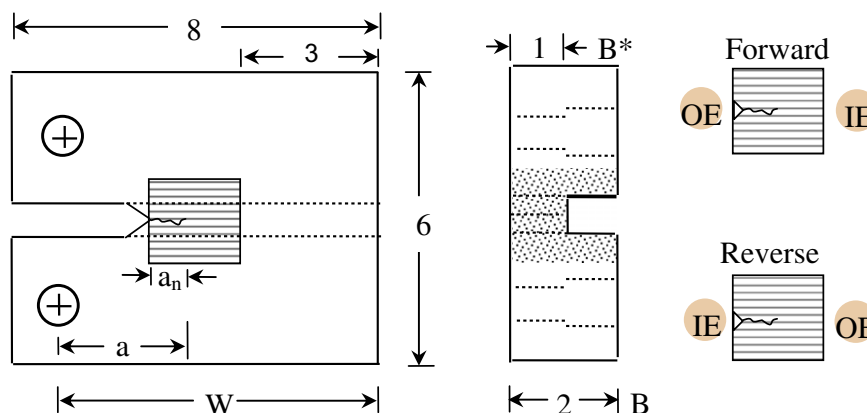


Fig. 2. Final geometry of the inset CT specimen (all dimensions in mm) and the two directions of crack extension.

followed by partial unloading and reloading. Digital images were acquired at the onset of loading, at the peak load, and at the end of the load decay to document the crack growth process. These procedures were followed until the crack reached a point of instability. DIC was then used to determine the full-field displacement distribution and to identify the crack tip from the location of zero opening displacement.

The opening mode stress intensity (K_I) distribution with crack extension was calculated according to Eq. (1). Resistance curves were obtained by plotting K_I and G_I^1 as a function of crack increment (Δa). Statistical differences within a group were calculated using the Grubb's test, whereas those between the groups were evaluated using a Student's t -test. Significant differences were identified by $p \leq 0.05$.

The fracture surfaces of all specimens were examined by scanning electron microscopy (SEM) with a JEOL JSM 5600 (JEOL Inc., Peabody, MA) in secondary electron imaging (SEI) mode. Cyclic crack extension was stopped prior to fracture in one specimen from each group; the crack face was etched using 34% phosphoric acid for 5 s and then coated with gold–palladium. Structural evaluation of these specimens was conducted using the scanning electron microscope in backscatter imaging (BSI) mode to identify the influence of microstructure of enamel on the crack growth behavior.

3. Results

3.1. Fatigue crack growth

A representative fatigue crack growth response in the forward direction is shown in Fig. 3. Crack arrest occurred frequently during the initial onset of growth and required an increase in the cyclic load to sustain cyclic extension. Such periodic acceleration and deceleration of a crack is characteristic of a “short” crack² response as denoted by the dotted line in Fig. 3. Further propagation lead to development of steady-state “long” crack³ behavior as represented by the solid line in this figure. Short crack growth behavior was also noted in the responses for fatigue crack

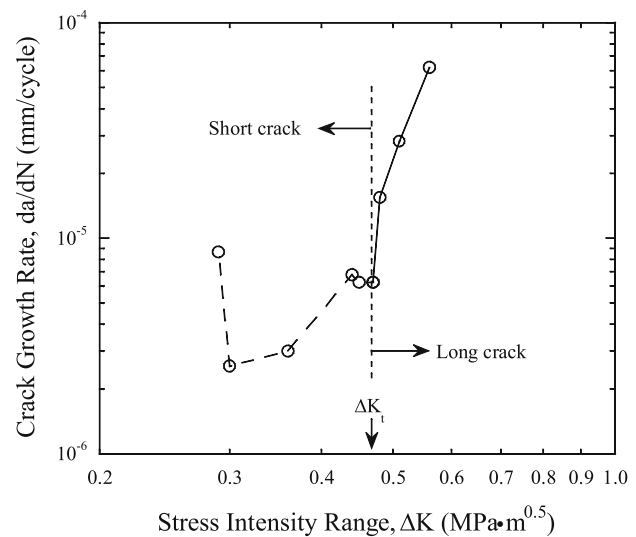


Fig. 3. Fatigue crack growth response in the forward direction. Initial crack growth resulted in periodic acceleration and deceleration and is representative of short crack behavior (dotted line). Subsequent growth resulted in steady-state “long” crack responses (solid line). A transition stress intensity range (ΔK_t) was defined for transition from the short to long crack regime.

growth in the reverse direction. However, subsequent growth in this orientation resulted in unstable cracking, and generally without development of long crack behavior. Cyclic crack growth is generally characterized using the Paris law, and has recently been used in quantifying fatigue crack growth in enamel [22]. However, the Paris law is not applicable for characterizing non-linear cyclic extension in the short crack regime of the forward direction or for the reverse direction. In turn, simple quantitative descriptions of the growth behavior in the two directions were used and the results are listed in Tables 1 and 2, respectively.

Cumulative fatigue crack growth responses for the forward and reverse directions are shown as a function of crack length and stress intensity range in Fig. 4a and b, respectively. Crack initiation in the outer enamel occurred over a lower stress intensity range ($\Delta K_o = 0.39 \pm 0.09 \text{ MPa m}^{0.5}$) compared to that in the inner enamel ($\Delta K_o = 0.53 \pm 0.12 \text{ MPa m}^{0.5}$). Stable crack growth in the forward direction extended more than 1.2 mm in length over a growth rate ranging from 1.7×10^{-7} to $6.2 \times 10^{-5} \text{ mm cycle}^{-1}$ and over an average ΔK ranging from 0.39 ± 0.09 to $0.65 \pm 0.14 \text{ MPa m}^{0.5}$. In the short crack regime, cyclic growth occurred over an average ΔK of 0.39 ± 0.09 to $0.49 \pm 0.11 \text{ MPa m}^{0.5}$ with corresponding growth rates in the range of 1.7×10^{-7} to $1.5 \times 10^{-5} \text{ mm cycle}^{-1}$. Subsequent growth resulted in a clear transition from short to long crack behavior and the corresponding ΔK was defined as the transition stress intensity range (ΔK_t). For the forward direction the average ΔK_t is $0.49 \text{ MPa m}^{0.5}$. Steady-state crack growth in the long crack regime occurred over an average ΔK of 0.49 ± 0.11 to $0.65 \pm 0.14 \text{ MPa m}^{0.5}$ with rates in the range of 1.0×10^{-6} to $6.2 \times 10^{-5} \text{ mm cycle}^{-1}$.

¹ The strain energy release rate for monotonic crack growth can be estimated as $G_I = K_I^2/E'$, where E' is the elastic modulus. E' for enamel is a function of distance from the DEJ and was obtained from Park et al. [33].

² Short cracks are defined as ones that are (i) comparable to the microstructural dimension of the material, (ii) smaller in length than the size of the plastic zone or (iii) when they are comparable to the extent of the zone of crack-tip shielding behind the crack tip [34]. In the present study the increment of crack extension is comparable to a few prism dimensions and is typically less than or comparable to the apparent shielding zone.

³ Long cracks have been traditionally described as those having a fully developed shielding zone and can be characterized by using linear elastic fracture mechanics (LEFM) [34]. In the present study the cracks that exhibit a continuous and steady increase in growth rate over an applied stress intensity range as shown in Fig. 3 are defined as long cracks.

Table 1

Summary of crack growth in the forward direction. The crack lengths are defined here from the notch (a_n) and include the length at initiation (a_o), at the transition from the short to the long crack regime (a_t) and at instability (a_c). The corresponding values of stress intensity range (ΔK_o , ΔK_t , ΔK_c) are also presented.

Age/gender	Initiation		Growth			
	a_o (μm)	ΔK_o MPa m ^{0.5}	Short crack		Long crack	
	a_o (μm)	ΔK_o MPa m ^{0.5}	a_t (μm)	ΔK_t MPa m ^{0.5}	a_c (μm)	ΔK_c MPa m ^{0.5}
27/F	450	0.47	650	0.52	1100	0.78
27/F	580	0.48	650	0.52	920	0.63
17/M	400	0.29	960	0.47	1220	0.56
18/F	680	0.40	890	0.50	1200	0.61
18/F	300	0.24	480	0.34	1220	0.63
19/M	600	0.37	–	–	950	0.45
23/F	440	0.47	490	0.68	880	0.87
Avg = 21 ± 4	493 ± 132	0.39 ± 0.09	687 ± 200	0.49 ± 0.11	1070 ± 150	0.65 ± 0.14

Table 2

Summary of crack growth in the reverse direction.

Age/gender	Initiation		Growth			
	a_o (μm)	ΔK_o MPa m ^{0.5}	Short crack		Long crack	
	a_o (μm)	ΔK_o MPa m ^{0.5}	a_t (μm)	ΔK_t MPa m ^{0.5}	a_c (μm)	ΔK_c MPa m ^{0.5}
22/F	260	0.45	670	0.6	–	0.6
18/M	140	0.51	344	0.57	–	0.57
22/F	140	0.37	580	0.51	–	0.51
18/M	95	0.46	205	0.63	297	0.65
22/F	171	0.59	320	0.75	–	0.75
18/M	97	0.68	600	0.86	–	0.86
18/M	114	0.68	511	0.85	–	0.85
Avg = 20 ± 2	145 ± 57	0.53 ± 0.12	461 ± 173	0.67 ± 0.15	–	0.68 ± 0.14

In the reverse direction stable crack extension occurred over less than 0.7 mm and proceeded at growth rates ranging from 6.7×10^{-8} to 3.8×10^{-5} mm cycle⁻¹, and over an average ΔK ranging from 0.53 ± 0.12 to 0.68 ± 0.14 MPa m^{0.5} (Fig. 4b). The responses primarily exhibited short crack behavior. The apparent ΔK_t for this orientation (0.67 MPa m^{0.5}) was equivalent to the stress intensity range at crack instability ($\Delta K_c = 0.68$ MPa m^{0.5}). Although crack growth in the forward direction transitioned from short crack to long crack behavior, cyclic crack growth in the reverse direction occurred exclusively in the short crack regime with subsequent growth resulting in unstable fracture.

3.2. Resistance–curve behavior

A typical load vs. load-line displacement curve for quasi-static crack growth in the two directions is shown in Fig. 5, which highlights pre-loading (Region I) and incremental crack extension (Region II). For growth in the forward direction, crack initiation typically occurred between 4 and 5 N. However, further crack extension required a steady increase in the driving force until reaching the point of instability. In comparison to fatigue crack growth, monotonic growth in the forward direction occurred over a longer length of extension up to 1.6 mm. The resulting stress intensity distribution for growth in

the forward direction (i.e. R-curve) exhibited a rise with crack extension (Fig. 6). The parameters used for quantifying the R-curves in the forward direction are listed in Table 3. The average initiation (K_o) and fracture (K_c) toughness was 0.55 ± 0.06 and 2.11 ± 0.20 MPa m^{0.5}, respectively. For crack growth in this configuration the strain energy release rate (G_I) (Fig. 6b) increased from nearly 4 J m⁻² at initiation to over 60 J m⁻² at fracture.

Crack initiation in the reverse direction required higher loads than in forward crack growth, typically between 6 and 8 N. Stable crack growth could not be reached in this configuration as the driving forces were large enough to cause unstable fracture. The growth parameters are listed in Table 4. There was no significant ($p > 0.05$) increase in toughness from initiation ($K_o = 0.87 \pm 0.13$ MPa m^{0.5}, $G_o = 10.0 \pm 2.1$ J m⁻²) to fracture ($K_c = 1.17 \pm 0.13$ MPa m^{0.5}, $G_c = 18.6 \pm 6.7$ J m⁻²).

3.3. Crack growth observations

A typical path of crack extension within an enamel inset in the forward direction is shown in Fig. 7. The crack morphology (Fig. 7a) exhibits two distinct characteristics. In the outer enamel crack growth occurs over a relatively straight path, whereas in the inner enamel the path is rather torturous in nature. At higher magnification the crack path revealed strong influence of the microstructure. Crack

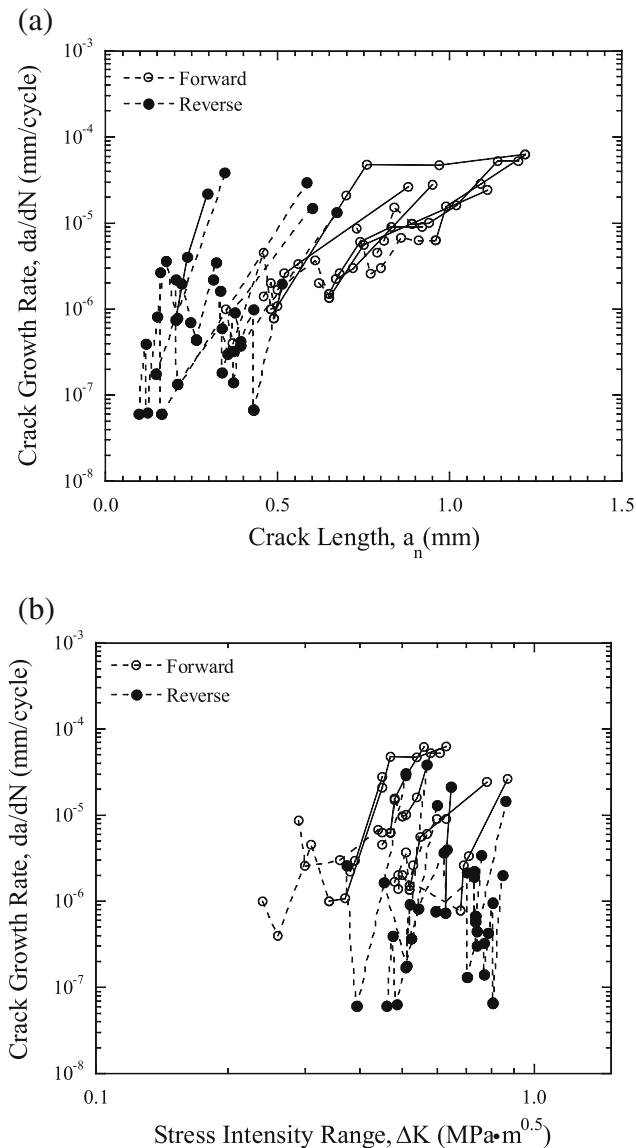


Fig. 4. Fatigue crack growth responses for the forward and reverse directions. Dotted lines indicate short cracks and solid lines indicate long cracks. (a) Incremental crack growth rate (da/dN) as a function of crack length (a_n). Note that stable crack growth in the forward direction occurred over a much longer length than in the reverse direction. (b) Incremental crack growth rate (da/dN) as a function of stress intensity range (ΔK). Note that crack growth in the reverse direction occurred mostly in the short crack regime with no stable transition to long crack behavior, whereas growth in the forward direction transitioned from short crack to long crack behavior with stable extension.

extension in the outer enamel occurred almost entirely between and parallel to the prisms (Fig. 7b). Growth at the transition from the outer to the inner enamel resulted in crack bifurcation (Fig. 7c), whereas growth within the complex microstructure (decussation) of the inner enamel was accompanied by a number of toughening mechanisms including bridging induced by unbroken ligaments of the tissue (Fig. 7d) and crack deflection (Fig. 7e). In addition, crack growth in the decussated region was accompanied by microcracking (Fig. 8a) about the primary crack and liga-

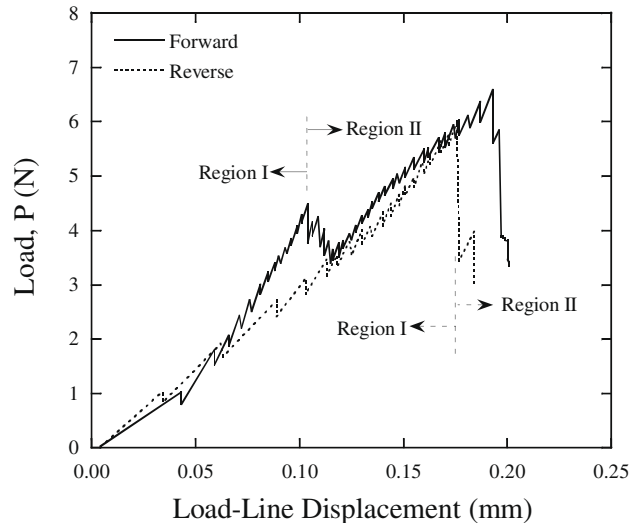


Fig. 5. A load vs. load-line displacement distribution for forward and reverse growth obtained during stable crack extension within enamel. Region I denotes preloading and Region II distinguishes the portion of response associated with incremental crack extension. Crack growth in the reverse direction resulted in unstable fracture, whereas stable crack growth in the forward direction required incremental increases in the driving force.

ments of organic matter bridging the crack (Fig. 8b). Several small broken tethers of organic material were evident on the fracture surface in the inner enamel (Fig. 8c). All these mechanisms were also active during crack extension in the reverse direction (Fig. 9). However, extrinsic mechanisms in the reverse direction evolved only for growth within the inner enamel and were not evident for growth in the outer enamel. When compared to growth in the forward direction, the potency of these toughening mechanisms was graded in the opposite direction as evident from the incremental crack growth responses in Figs. 4 and 6.

4. Discussion

A comparison of responses for fatigue crack growth showed that the inner enamel exhibited significantly higher ($p < 0.05$) resistance ($\Delta K_o = 0.53 \pm 0.12 \text{ MPa m}^{0.5}$) to the initiation of cyclic extension than the outer enamel ($\Delta K_o = 0.39 \pm 0.09 \text{ MPa m}^{0.5}$). Following initiation, crack growth in both directions exhibited short crack behavior where small cracks equivalent to a few prism dimensions underwent retardation. Cyclic extension in the short crack regime for the reverse direction occurred over lower growth rates in comparison to the forward direction. However, a transition from short to long crack cyclic extension resulted in stable growth in the forward direction only. Overall, stable crack growth extended over longer crack lengths in the forward direction (Fig. 4a, Table 1) and over a ΔK approximately twice that in the reverse direction (Fig. 4b, Table 2).

Results from the monotonic crack growth experiments also showed that the initiation toughness of the inner

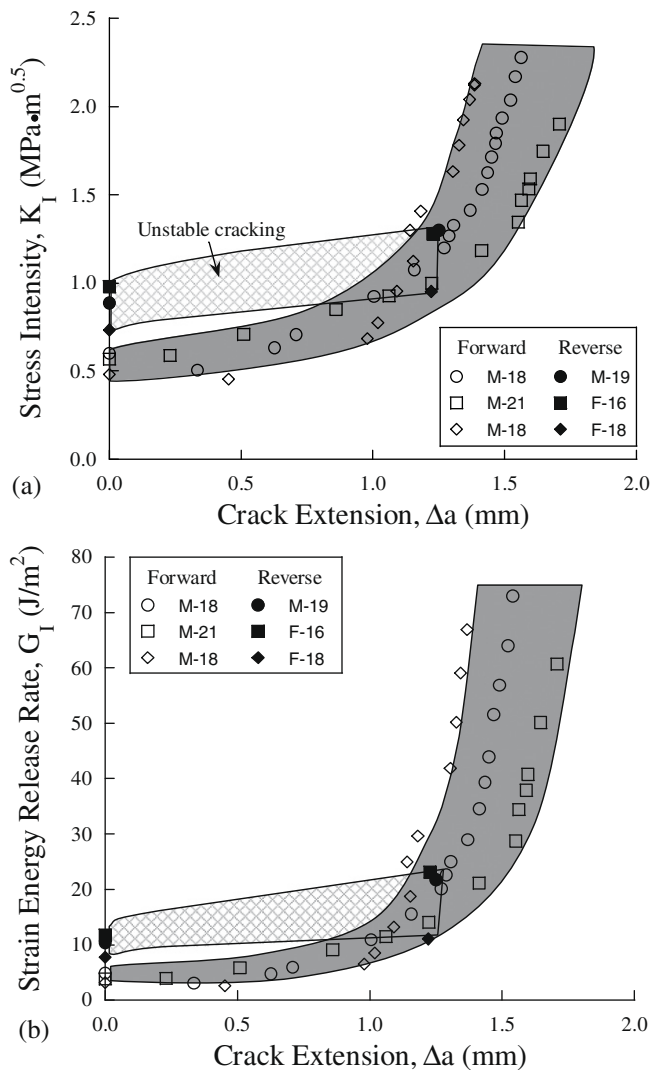


Fig. 6. Crack growth resistance curves for growth in the forward and reverse directions. (a) Stress intensity (K_I) plotted as a function of crack extension (Δa). (b) Strain energy release rate (G_I) plotted as a function of Δa . Crack growth in the forward direction resulted in rising R-curve behavior and a significant increase in G , whereas that in the reverse direction resulted in a small rise in toughness with unstable cracking.

Table 3
Crack growth resistance parameters for the forward direction.

Gender/age	Stress intensity range ($\text{MPa m}^{0.5}$)		Strain energy release rate (J m^{-2})	
	Initiation K_o	Fracture K_c	Initiation G_o	Fracture G_c
M/18	0.60	2.30	4.9	72.9
M/21	0.57	1.90	3.8	60.7
M/18	0.48	2.13	3.2	66.9
Avg	0.55 ± 0.06	2.11 ± 0.20	4.0 ± 0.9	66.8 ± 6.1

Table 4
Crack growth resistance parameters for the reverse direction.

Gender/age	Stress intensity range ($\text{MPa m}^{0.5}$)		Strain energy release rate (J m^{-2})	
	Initiation K_o	Fracture K_c	Initiation G_o	Fracture G_c
M/19	0.89	1.30	10.4	21.7
F/16	0.98	1.27	11.8	23.2
F/18	0.73	0.95	7.7	11.0
Avg	0.87 ± 0.13	1.17 ± 0.13	10.0 ± 2.1	18.6 ± 6.7

enamel ($K_o = 0.87 \pm 0.13 \text{ MPa m}^{0.5}$) was significantly higher ($p < 0.05$) than that of the outer enamel ($K_o = 0.55 \pm 0.06 \text{ MPa m}^{0.5}$). However, crack growth in the forward direction was significantly more stable than in the reverse direction as distinguished from the rising R-curve responses (Fig. 6). Crack growth in the forward direction resulted in a 300% increase in toughness from initiation to fracture. This rise in toughness was primarily attributed to mechanisms identified within the inner enamel that consumed fracture energy. The resulting energy at fracture for forward crack growth ($G_c = 66.8 \pm 6.1 \text{ J m}^{-2}$) was more than 15 times higher than that at initiation ($G_o = 4.0 \pm 0.9 \text{ J m}^{-2}$). In comparison, crack growth in the reverse direction was far less stable and resulted in approximately 30% increase in K_I over the total growth path. The total energy consumed in fracture of enamel in the reverse direction ($G_c = 18.6 \text{ J m}^{-2}$) is less than a third of that consumed in the forward direction.

Both the fatigue and monotonic crack growth responses of the enamel were most stable in the forward direction. This behavior can be directly linked to the microstructural arrangement of prisms. For instance, cyclic crack growth through the straight prisms of the outer enamel underwent retardation when the crack reached the complex crossing of the prisms in the decussated region (Fig. 7). Initial stability is often achieved by crack bifurcation in the order of tens of micrometers resulting at the transition of the outer and the inner enamel (Fig. 7c). The stability of cracks growing towards the DEJ is attributed to a combination of extrinsic mechanisms such as crack deflection and crack bridging that develops and evolves with crack extension throughout the decussated enamel (Fig. 7). While unbroken ligaments of enamel are formed by cracks propagating through the complex intertwined prisms (Fig. 7d), crack deflection results from a relative change in prism orientation (Fig. 7e). A combination of these mechanisms resulted in a substantial increase in toughness via crack closure and reduction in the local stress intensity at the crack tip. In the reverse direction these mechanisms also contribute to crack

growth resistance in the decussated enamel. For example, cracks extending from near the DEJ experienced curving along the weak interprismatic boundaries of the oblique prisms (Fig. 9b) and crack bridging in the decussated enamel (Fig. 9d), thereby causing deceleration of the crack. However, subsequent growth towards the outer enamel resulted in no further evolution of such toughening mechanisms due to relatively straight prism orientation and a reduction in contribution from the existing ones. With reduction of these energy dissipating mechanisms the crack

undergoes higher growth rates over the applied stress intensity range and reaches instability at shorter crack lengths.

In addition to the toughening mechanisms documented in Figs. 7 and 9, crack growth retardation was partially achieved by microcracking/loosening of the interprismatic boundaries in the *K* dominant zone. Evidence of such interprismatic loosening was noted by the ingress and egress of fluid in fatigue (Fig. 8a) around the main crack, and was most prominent in the inner enamel. Similar observations have been reported for crack growth in dentin [35] and

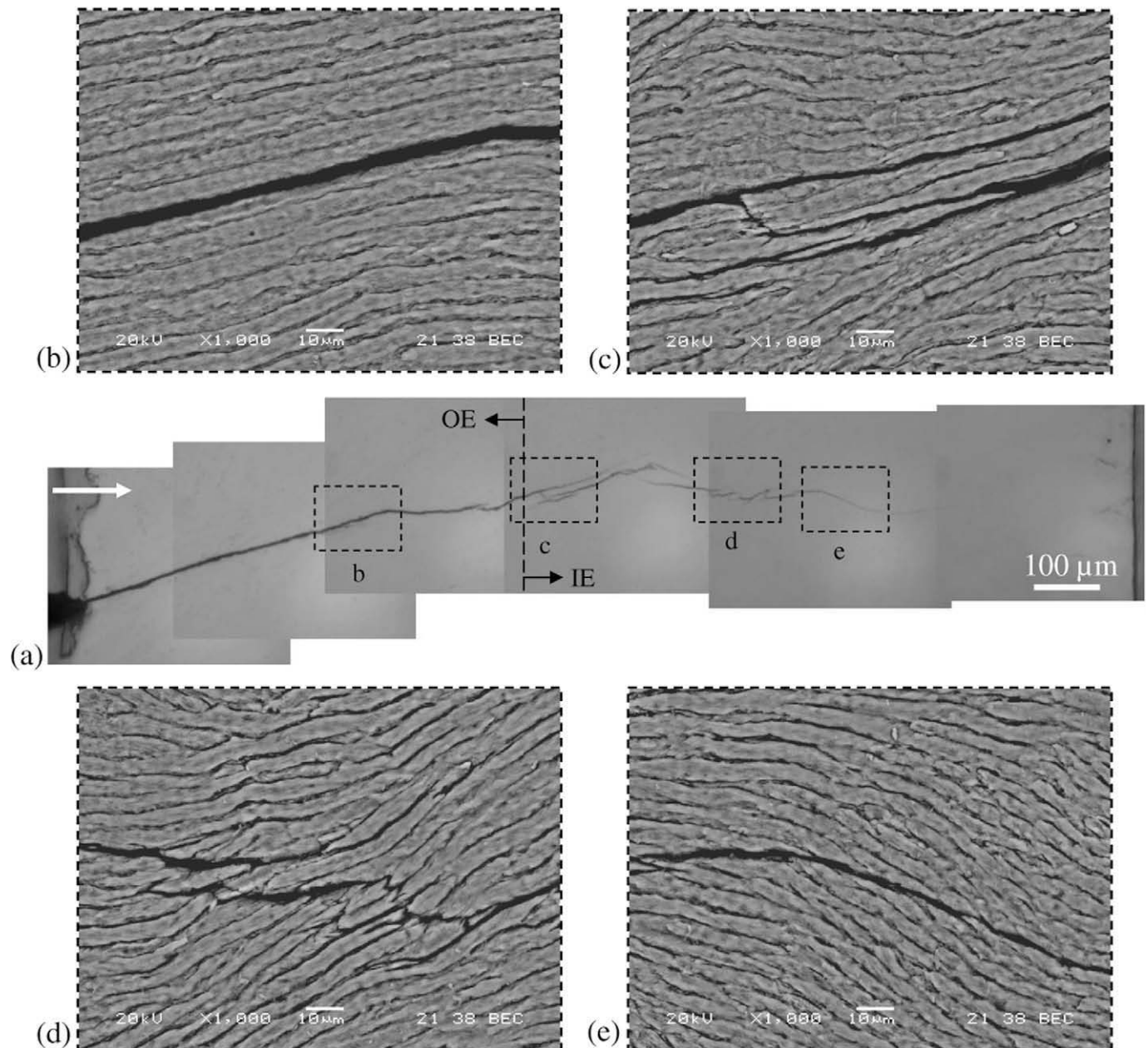


Fig. 7. Observations of crack growth in the forward direction. Direction of crack growth is from left to right indicated by white arrow. (a) Optical micrograph of crack extension showing straight crack growth in the enamel. Crack growth in the inner enamel was accompanied by various mechanisms of toughening. (b) Straight crack path in the outer enamel is attributed to the relatively straight prism orientation. The microstructure guides the crack towards the inner enamel. (c) Crack bifurcation occurred while transitioning from the outer to the inner enamel. (d) Crack extension through the decussated zone resulted in formation of unbroken ligament bridges. (e) Crack growth in the proximity of the DEJ underwent deflection and stall due to change in prism orientation. Note that the data for this specimen was corrected for crack deflection in the outer enamel.

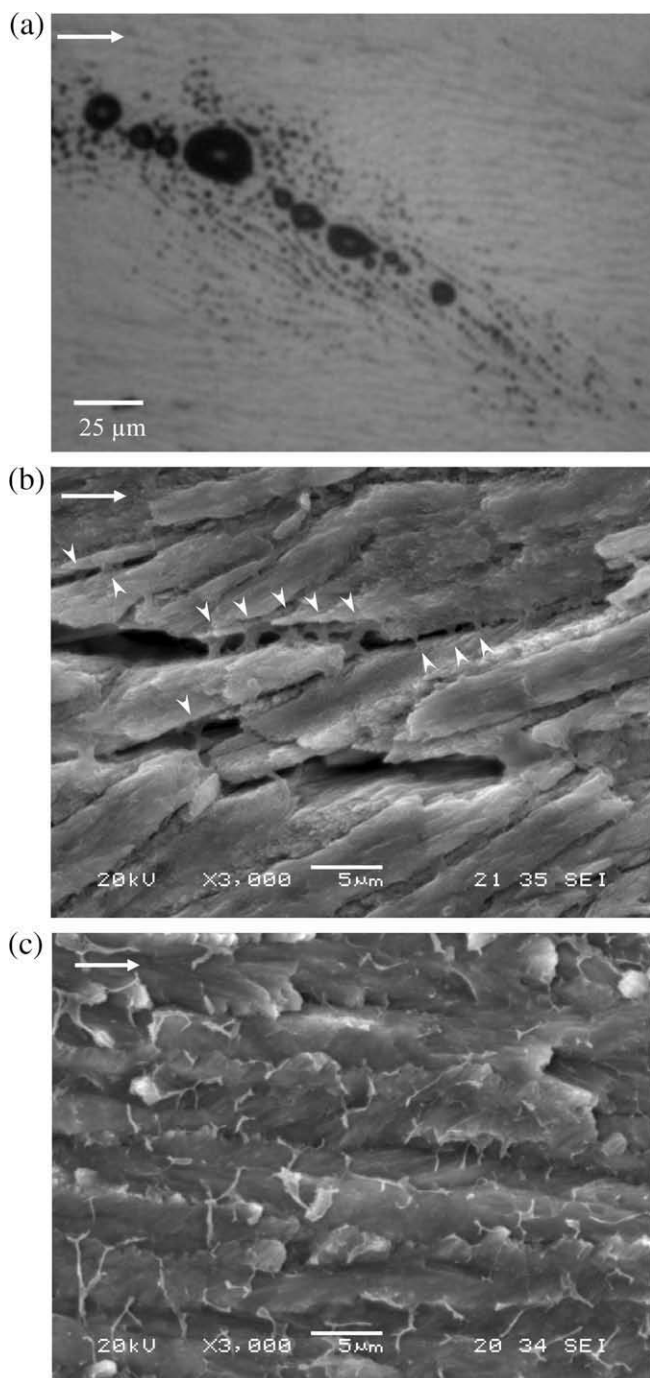


Fig. 8. Observations of microcracking and organic bridging. (a) Optical micrograph of HBSS droplets developed around the crack during cyclic loading. The larger bubbles in the figure show fluid pushed out of the main crack whereas the smaller droplets result from loosening of interprismatic spaces adjacent to the crack. (b) Crack growth in the decussated enamel resulted in the formation of ligament bridges (white arrowheads) of organic material. (c) Evidence of fractured organic ligaments on the fracture surface. Such observations were commonly made in the enamel near the proximity of the DEJ.

result in an inelastic zone around the crack tip. A first-order estimate of the microcracking zone in enamel can be obtained from the observations of fluid movement (Fig. 8a), which spanned a distance of approximately

50 μm about the crack, resulting in an inelastic zone height of ~25 μm. Note that the extent of interprismatic loosening is expected to scale according to the volume fraction of organic matter within the K dominant region. Therefore, with an increase in the organic content in the proximity of the DEJ [10] the toughening associated with non-linear processes would be expected to increase. An estimate of the organic content can be obtained by examining the gradient of elastic modulus from the outer to the inner enamel. According to Gao et al. [36], the elastic modulus of a biocomposite is a function of its mineral constituent embedded in the organic matrix and can be estimated from:

$$\frac{1}{E} = \frac{4(1-\phi)}{\mu_p \phi^2 \rho^2} + \frac{1}{\phi E_m}, \quad (2)$$

where E is the effective Young's modulus, ϕ is the volume fraction of mineral, μ_p is the shear modulus of protein (~0.1 GPa [37]), ρ is the aspect ratio of mineral particles (~30–50 for enamel [38,39]) and E_m is the Young's modulus of the mineral (~114 GPa for hydroxyapatite [37,40]). Substituting for these values in Eq. (2) and considering the gradient in elastic modulus from outer ($E = 90$ GPa) to inner enamel ($E = 70$ GPa) [33] results in an approximate volume fraction increase in the organic component from 4% in the outer enamel to 10% near the DEJ. Therefore, the expected degree of interprismatic loosening about the crack in the inner enamel would be over two times that contributing to crack tip shielding in the outer enamel.

In addition to the aforementioned contribution of the organic matrix, proteins have been shown to impart back-creep [41], promote anti-fatigue [42] and contribute to crack arrest [40]. When a crack traverses along the prism boundaries the interprismatic protein resists the separation of the prisms by forming secondary tethers (Fig. 8b). Bridging imposed by the organic matrix promotes closure stresses over the extent of unfolding, which can be active for relatively large crack opening displacements (on the order of a few micrometers) [43]. Energy dissipation promoted by unfolding and rupture of these sacrificial bonds (Fig. 8c) increases the driving force required for a crack to propagate, thereby increasing the crack growth resistance and the apparent toughness of enamel. Such bonding and development of tethers can occur at even smaller length scales, i.e. between the individual hydroxyapatite nanocrystals [37]. A simple estimate of fracture energy (J_c) of a biocomposite (such as enamel) consumed by these tethers can be obtained from [44]:

$$J_c = \xi(1-\phi)L\varepsilon_p\tau_p, \quad (3)$$

where L is the length of the mineral crystal, ε_p is the effective strain of protein before fracture, ξ is a geometric factor (≥ 1 [44]), and the quantity $(1-\phi)$ represents the volume fraction of organic material. Assuming ξ , L , ε_p and τ_p to be constant throughout the enamel thickness, the increase in organic content with depth from enamel (computed from Eq. (2)) would promote an increase in the fracture

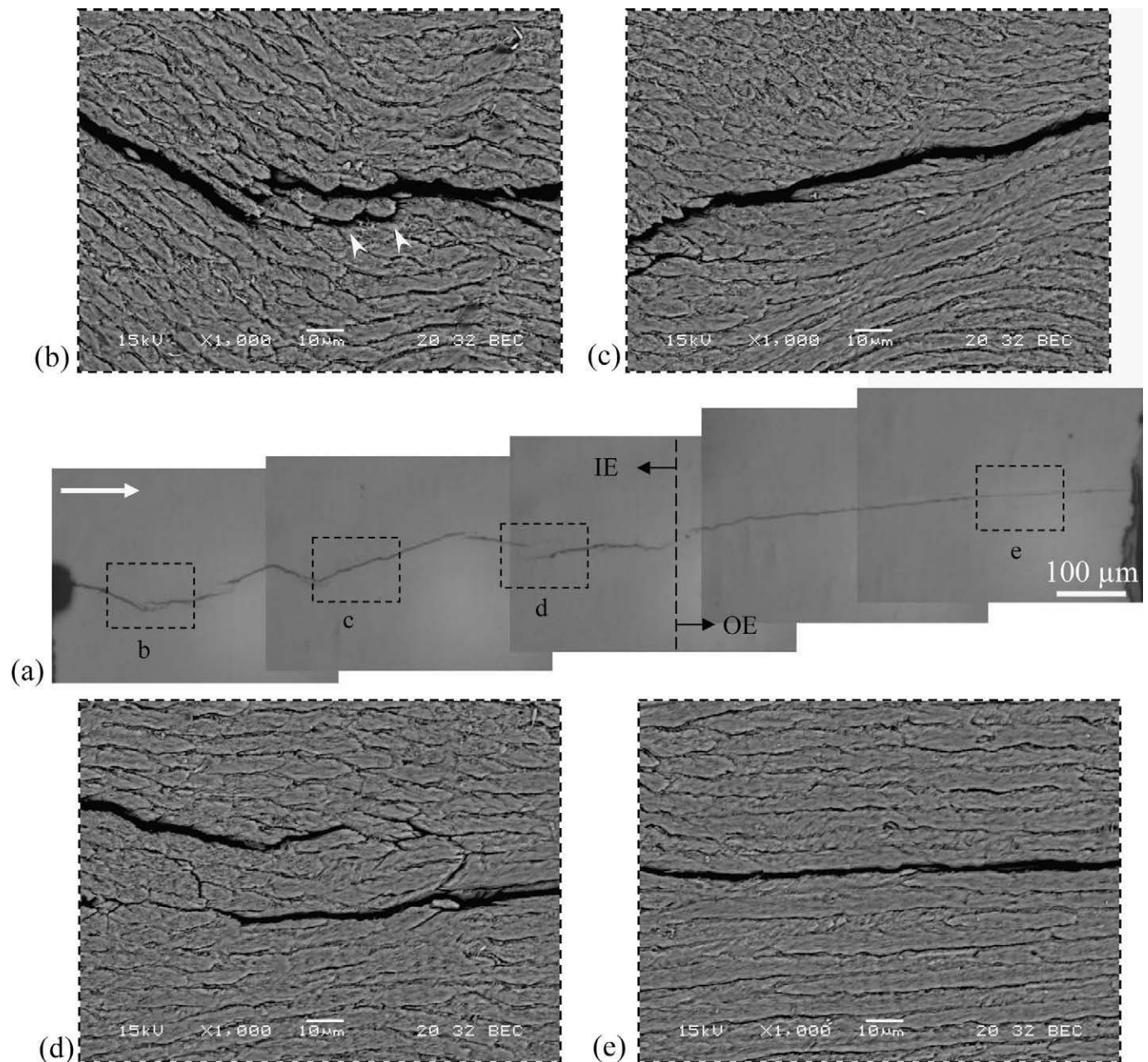


Fig. 9. Observations of crack growth in the reverse direction. Direction of crack growth is from left to right. (a) An optical micrograph of crack extension from inner to outer enamel. (b) Cyclic crack growth within the inner enamel resulted in crack curving (white arrowheads) along the interprismatic boundary of oblique prisms in the decussated zone, (c) followed by crack deflection due to change in prism orientation. (d) Crack growth in the decussated enamel was also accompanied by formation of few unbroken ligaments of tissue bridging the crack. (e) Crack growth in the outer enamel resulted in unsteady growth due to relatively straight prism orientation and no further evolution of toughening mechanisms.

energy dissipated due to protein domain unfolding by over a factor of 2. Though the energy consumed due to protein bridging is expected to be less than 10% of the total energy required for fracture, deformation of the protein serves as a precursor for microcracking and crack bridging—the two major energy-dissipating mechanisms. Thus, the increase in protein content with proximity to the DEJ serves an important role in the toughening behavior, particularly in the forward direction.

Results from the present experimental evaluation showed that the arrangement of prisms and the organic

matrix in enamel is critically important to the crack growth resistance of this highly mineralized tissue. Crack growth in the forward direction is guided by the prisms towards the less brittle inner enamel, where they experience increasing growth resistance due to host of mechanisms operating from the meso- to the nano-scale. The evolution of such processes is facilitated (at least in part) by the higher organic content in the inner enamel (as shown by Eqs. (2) and (3)). From a mechanistic point of view, the results justify nature's choice of incorporating the complex structure only in the inner enamel as contact damage can be

guided to prevent deflection back to the tooth's surface, thereby preventing the development of deleterious chips.

Contact-induced cracking of enamel is not limited to initiation from the occlusal surface. Radial cracks may develop at the DEJ and propagate from the inner enamel outwards [46]. While the highly graded microstructure of the inner enamel will promote higher initiation resistance and result in lower cyclic growth rates of these radial cracks, they will reach instability after less than half the length of extension in the forward direction, and with far lower energy⁴ required for fracture. This means that human enamel is far less resistant to fracture from “internal” radial cracks, similar to that in the core of all ceramic dental crowns. Results from the present study suggest that the structure of human enamel is optimized for resisting and arresting crack growth in the forward direction. This “unidirectional anisotropy” in crack growth resistance exhibited by enamel is novel and not exhibited in the mechanical behavior of engineered materials. As such, the guided crack growth and arrest characteristics presented in this paper offer new insight towards the development of tougher dental ceramics and multifunctional hybrid materials.

5. Conclusions

An evaluation of fatigue and monotonic crack growth in human enamel was performed using an inset CT specimen. Cracks were grown in both forward and reverse directions to examine the importance of microstructural variations on the crack growth resistance. The following conclusions were drawn:

- (1) The fatigue crack growth responses exhibited short crack behavior in both directions. However, steady-state long crack behavior was exhibited by cracks extending in the forward direction only. The resulting extent of stable crack growth in the forward direction was approximately twice that achieved for the reverse direction, and also occurred over a stress intensity range twice that in the reverse direction.
- (2) Monotonic crack growth in the forward direction resulted in a rising R-curve with a 300% increase in toughness and an increase in G from near 4 J m^{-2} at initiation to over 60 J m^{-2} at fracture. The rise in toughness with crack extension was most significant in the inner enamel. Crack growth in the reverse direction was less stable, resulting in about 30% increase in toughness and an insignificant rise in G from initiation (10 J m^{-2}) to fracture (18.6 J m^{-2}).

⁴ Note that in the present study fracture energy is represented in the form of energy release rate (G) and is deduced from K obtained using LEFM. Since the contributions due to inelastic deformation would increase in the inner enamel, the use of J , which is the energy associated with inelastic deformation, would be more appropriate [45].

Overall, the total energy absorbed during crack growth in the forward direction was over three times higher than that in the reverse direction.

- (3) Crack growth toughening occurred in both directions and was promoted by a combination of crack bridging, crack deflection and crack bifurcation. The organic matter at the prism boundaries was found to play a unique role in imparting crack growth retardation through the formation of several unbroken tethers and microcracking induced by loosening of the prisms. The potency of such mechanisms was shown to increase in the forward direction due to a corresponding increase in the organic content.
- (4) The microstructure of enamel is functionally optimized to guide cracks from the more brittle outer enamel inwards where they experience higher growth resistance and are prevented from causing fracture and chipping.

Acknowledgments

This work was supported in part by the NIDCR (DE016904) and the NSF (BES0521467). The authors would like to thank Ultradent Products Inc. for supplying the Vit-l-escence resin composite and Dr. Judith Porter of the University of Maryland, Baltimore for bonding supplies.

References

- [1] Ellyin F. Fatigue damage, crack growth and life prediction. London: Chapman and Hall; 1997.
- [2] Frost HM. Transient-steady state phenomenon in microdamage physiology: a proposed algorithm for lamellar bone. *Calcif Tissue Int* 1989;44:367–81.
- [3] Burr DB. Bone, exercise and stress fractures. *Exerc Sport Sci Rev* 1997;25:171–94.
- [4] Taylor D. Failure processes in hard and soft tissues. In: Milne I, Ritchie RO, Karihaloo B, editors. *Comprehensive structural integrity: fracture of materials from nano to macro*, vol. 9. Oxford: Elsevier; 2003. p. 35–95.
- [5] Kaewsuriyathumrong C, Soma K. Stress of tooth and PDL structure created by bite force. *Bull Tokyo Med Dent Univ* 1993;40:217–32.
- [6] Burke FJT. Tooth fracture in vivo and in vitro. *J Dent* 1992;20:131–9.
- [7] Taylor D. Fracture and repair of bone: a multiscale problem. *J Mater Sci* 2007;42:8911–8.
- [8] Curry JD. The design of mineralized hard tissues for their mechanical functions. *J Exp Biol* 1999;202:3285–94.
- [9] Popowics TE, Rensberger JM, Herring SW. Enamel microstructure and microstrain in the fracture of human and pig molar cusps. *Arch Oral Biol* 2004;49:595–605.
- [10] Ten Cate AR. *Oral Histology: development, structure and function*, vol. 5. St. Louis, MO: Mosby; 1998.
- [11] White SN, Luo W, Paine ML, Fong H, Sarikaya M, Snead ML. Biological organization of hydroxyapatite crystallites into a fibrous continuum toughens and controls anisotropy in human enamel. *J Dent Res* 2001;80:321–6.
- [12] Rensberger JM. Pathway to functional differentiation in mammalian enamel. In: Teaford MF, Smith MM, Ferguson MWJ, editors. *Development, function and evolution of teeth*. Cambridge: Cambridge University Press; 2000.

- [13] Vashishth D, Behiri J, Bonfield J. Crack growth resistance in cortical bone: concept of microcrack toughening. *J Biomech* 1997;30:763–9.
- [14] Akkus O, Rimnac CM. Cortical bone tissue resists fatigue fracture by deceleration and arrest of microcrack growth. *J Biomech* 2001;34:757–64.
- [15] Nalla RK, Kruzic JJ, Kinney JH, Ritchie RO. Mechanistic aspects of fracture and R-curve behavior in human cortical bone. *Biomaterials* 2005;26:217–31.
- [16] O'Brien FJ, Taylor D, Clive Lee T. The effect of bone microstructure on the initiation and growth of microcracks. *J Orthop Res* 2005;23:475–80.
- [17] Koester KJ, Ager 3rd JW, Ritchie RO. The true toughness of human cortical bone measured with realistically short cracks. *Nat Mater* 2008;7:672–7.
- [18] Kruzic JJ, Nalla RK, Kinney JH, Ritchie RO. Mechanistic aspects of in vitro fatigue-crack growth in dentin. *Biomaterials* 2005;26:1195–204.
- [19] Bajaj D, Sundaram N, Nazari A, Arola D. Age, dehydration and fatigue crack growth in dentin. *Biomaterials* 2006;27:2507–17.
- [20] Arola D, Reid J, Cox ME, Bajaj D, Sundaram N, Romberg E. Transition behavior in fatigue of human dentin: structure and anisotropy. *Biomaterials* 2007;28:3867–75.
- [21] Nazari A, Bajaj D, Zhang D, Romberg E, Arola D. Aging and the reduction in fracture toughness of dentin. *J Mech Behav Biomed Mater* 2009; doi:10.1016/j.jmbbm.2009.01.008.
- [22] Bajaj D, Nazari A, Eidelman N, Arola D. A comparison of fatigue crack growth in human enamel and hydroxyapatite. *Biomaterials* 2008;29:4847–54.
- [23] Rasmussen ST, Patchin RE. Fracture properties of human enamel in an aqueous environment. *J Dent Res* 1984;63:1362–8.
- [24] Bajaj D, Arola D. On the R-curve behavior of human tooth enamel. *Biomaterials*, in press. doi:10.1016/j.biomaterials.2009.04.017.
- [25] Skobe Z, Stern S. The pathway of enamel rods at the base of cusps of human teeth. *J Dent Res* 1980;59:1026–32.
- [26] Rensberger JM, Koenigswald WV. Functional and phylogenetic interpretation of enamel microstructure in rhinoceroses. *Paleobiology* 1980;6:477–95.
- [27] Fortelius M. Ungulate cheek teeth: developmental, functional, and evolutionary interrelations. *Acta Zoologica Fennica* 1985;180:1–76.
- [28] Rensberger JM. Adaptation of enamel microstructure to differences in stress intensity in the Eocene perissodactyl *Hyracotherium*. In: Kobayashi I, Mutvie H, Sahani A, editors. *Structure, formation and evolution of fossil hard tissues*. Tokyo: Tokai University Press; 1993. p. 131–45.
- [29] Curry JD. *Bone: structure and mechanics*. Princeton, NJ: Princeton University Press; 2002.
- [30] Zhang D, Nazari A, Soappman M, Bajaj D, Arola D. Methods for examining the fatigue and fracture behavior of hard tissues. *Exp Mech* 2007;47:325–36.
- [31] Soappman M, Nazari A, Porter JA, Arola D. A comparison of fatigue crack growth in resin composite, dentin and the interface. *Dent Mater* 2007;23:608–14.
- [32] Zhang D, Arola D. Application of digital image correlation to biological tissues. *J Biomed Opt* 2004;9:691–9.
- [33] Park S, Wang DH, Zhang D, Romberg E, Arola D. Mechanical properties of human enamel as a function of age and location in the tooth. *J Mater Sci Mater Med* 2008;19:2317–24.
- [34] Suresh S, Ritchie RO. Propagation of short fatigue cracks. *Int Met Rev* 1984;29:445–76.
- [35] Kahler B, Swain MV, Moule A. Fracture-toughening mechanisms responsible for differences in work to fracture of hydrated and dehydrated dentine. *J Biomech* 2003;36:229–37.
- [36] Gao H, Ji B, Jäger IL, Arzt E, Fratzl P. Materials become insensitive to flaws at nanoscale: lessons from nature. *Proc Natl Acad Sci USA* 2003;100:5597–600.
- [37] Xie Z, Swain M, Munroe P, Hoffman D. On the critical parameters that regulate the deformation behavior of tooth enamel. *Biomaterials* 2008;29:2697–703.
- [38] Daculsi G, Menanteau J, Jerebek LM, Mitre D. Length and shape of enamel crystals. *Calcif Tissue Int* 1984;36:550–5.
- [39] Kirkham J, Brookes SJ, Shore RC, Bonass WA, Smith DA, Wallwork ML, et al. Atomic force microscopy studies of crystal surface topology during enamel development. *Connect Tissue Res* 1998;38:91–100.
- [40] Ji B, Gao H. Mechanical properties of nanostructure of biological materials. *J Mech Phys Solids* 2004;52:1963–90.
- [41] He LH, Swain MV. Influence of environment on the mechanical behaviour of mature human enamel. *Biomaterials* 2007;28:4512–20.
- [42] He LH, Swain MV. Enamel—a “metallic-like” deformable biocomposites. *J Dent* 2007;35:431–7.
- [43] Rief M, Gautel M, Oesterhelt F, Fernandez J, Gaub H. Reversible unfolding of individual titin immunoglobulin domains by AFM. *Science* 1997;276:1109–12.
- [44] Gao H, Ji B, Buehler MJ, Yao H. Flaw tolerant bulk and surface nanostructures of biological systems. *Mech Chem Biosyst* 2004;1:37–52.
- [45] Anderson TL. *Fracture mechanics: fundamentals and applications*. 3rd ed. Boca Raton, FL: CRC Press; 2005.
- [46] Lawn BR, Lee JJ-W, Constantino PJ, Lucas PW. Predicting failure in mammalian enamel. *J Mech Behav Biomed Mater* 2009;2:33–42.